Dynamic 3D UAV Placement Optimization: Improved Bonobo Optimizer for Enhanced Coverage and Communication

Selma Yahia, Sylia Mekhmoukh Taleb, Valeria Loscri, Amylia Ait Saadi, Tu Dac Ho, Van Nhan Vo, Hossien Eldeeb, Sami Muhaidat

Dynamic 3D UAV Placement Optimization: Improved Bonobo Optimizer for Enhanced Coverage and Communication

Selma Yahia[1], Sylia Mekhmoukh Taleb[2], Valeria Loscri[1], Amylia Ait Saadi[3], Tu Dac Ho[4, 5], Van Nhan Vo[6, 7], Hossien Eldeeb[8], and Sami Muhaidat[8]
[1]Inria Lille- Nord Europe Lille, 59000 France
[2]LIST Laboratory, University of M'Hamed Bougara, 35000 Boumerdes, Algeria
[3]ESME Engineering School, 94200 Ivry-sur-Seine, France
[4]Department of Information Security and Communication Technology, Norwegian University of Science and Technology
[5]Department of Electrical Engineering, the Arctic University of Norway
[6] Faculty of Information Technology, Duy Tan University, Vietnam
[7]The Institute of Research and Development, Duy Tan University, Vietnam
[8]6G Research Center, Computer and Communication Engineering, Khalifa University, Abu Dhabi, UAE

***Abstract*—Unmanned aerial vehicles (UAVs) offer a promising solution for enhancing network coverage, reliability, and data speed in future wireless network generations. However, deploying UAVs as aerial base stations requires careful consideration of crucial design factors, including three-dimensional (3D) placement and performance optimization tailored to specific applications. In this paper, the 3D placement of multiple UAVs, acting as aerial base stations, is investigated in a dynamic user scenario. First, a closed-form expression for the coverage probability is derived. Then, to maximize the network coverage and sum rate while ensuring reliable and energy efficient system, a joint multi-objective optimization problem is formulated considering the real-time user movements. To solve the problem, an improved Chaos-based Bonobo Optimizer (CBO) scheme is proposed which combines chaotic maps with the Bonobo Optimizer (BO) algorithm. The obtained results demonstrate the superior performance of the proposed approach compared with different benchmark algorithms. The results reveal that the proposed CBO algorithm offers a minimum of 15% and 90 Mbit/s improvements in coverage and sum rate, respectively.**

***Index Terms*—Unmanned aerial vehicles, Improved Bonobo Optimizer, Coverage, 3D deployment.**

I. Introduction

The surge in mobile device usage has increased communication traffic and service demands in wireless networks. Inconsistent coverage, known as "coverage holes," remains an issue in many areas due to urban developments, natural disasters, and temporary events [1], [2]. Unmanned aerial vehicles (UAVs) offer a promising solution to address such challenges promptly, without a need for new ground-based base station (BS) establishment. That can significantly enhance the network efficiency while reducing the time for network deployment and startup. The mobility and adaptability of UAVs as well as their ability to establish line-of-sight (LoS) connections with ground users make them ideal for on-demand deployment, densely populated areas, and public safety services. However, to enhance the coverage and data rate, optimal design considerations for three-dimensional (3D) placement and tailored performance are crucial for UAV-assisted mobile wireless networks.

Numerous research endeavors have been dedicated to enhance the coverage of UAV-assisted networks by investigating optimal placement and effective deployment strategies for UAVs under the assumption of single-UAV networks. For instance, the works in [3], [4] presented UAV placement techniques to expand the coverage [3] or increase the number of users [4], respectively. The work in [5] focused on obtaining the optimal altitude that maximizes the coverage and minimizes the outage probability. In an attempt to consider the multiple UAVs case, the authors in [6]–[9] explored the potential UAVs deployments under the assumption of either fine-tuning the horizontal positioning of UAVs (keeping the altitude constant) [6] or optimizing the altitude but at a fixed horizontal stance [7]–[9]. Additionally, some recent works [10]–[12] have analyzed the coverage performance under the impact of small-scale fading in UAV communication systems. From our best knowledge, these studies often lack closed-form expressions for coverage probability.

Another critical factor that should be taken into account is the energy consumption required for UAV's hovering, traveling, and onboard components, which mainly affect UAV flight time and its connectivity with the users. To reflect this, the authors in [4], [13] introduced 3D UAVs deployments to minimize transmit power and enhance the energy efficiency. Other efforts to maximize network lifetime have considered factors such as optimal cooperative relaying schemes [14], bandwidth and energy efficiency trade-offs [15], and recharging operations [16]. However, none of these studies have fully captured the dynamic nature of UAVs deployment in response to real-time changes in user distribution and demand.

Motivated by this, this paper tackles the optimization

Fig. 1: Multi-UAVs-assisted wireless network.

challenge of 3D deployment for multiple UAVs in mobile wireless networks. The objective is to enhance the coverage performance, system reliability and sum rate while minimizing the energy consumption in dynamic scenarios. The proposed approach considers the trade-off between the benefits of UAV mobility for system adaptability and the associated energy expenditure. First, to model real-time user movement, we adopt a Random Waypoint (RWP) mobility model and derive a closed-form expression for coverage probability tailored to specific network requirements. Since balancing coverage enhancement, sum rate, and energy consumption is a complex task, a non-convex multi-objective optimization problem is then formulated. To effectively solve the problem, an enhanced Chaos-based Bonobo Optimizer (CBO) scheme is proposed that integrates chaotic maps into the original Bonobo Optimizer (BO). Finally, the coverage and sum rate performance of the proposed CBO scheme is compared with different benchmarks, including BO, Particle Swarm Optimization (PSO), and Bat Algorithm (BA) schemes.

The paper is structured as follows. Section II presents the system and channel modeling of 3D UAVs network. Section III discusses the performance metrics and derives the coverage. Section IV optimizes the system performance introducing a novel enhanced CBO scheme. Numerical results and comparisons with other algorithms are presented in Section V. The paper is finally concluded in Section VI.

II. System and Channel Models

A. Dynamic Scenario Under Consideration

Figure 1 depicts the multi-UAV network under consideration wherein a set of $\mathcal{M} = \{1, 2, \ldots, M\}$ drones operate as aerial base stations, providing connectivity services to a set of $\mathcal{N} = \{1, 2, \ldots, N\}$ terrestrial users, referred to as ground users (GUs). Within the 3D Cartesian coordinate framework, the position of the i^{th} UAV, $i \in \mathcal{M}$ is specified by coordinates (X_i, Y_i, H_i), while the j^{th} GU, $j \in \mathcal{N}$ is located at (X_j, Y_j, H_j). All UAVs hover at an altitude $H_i > 0$, and GUs are assumed to be at ground level with $H_j = 0$.

In this study, the GUs are mobile according to the Random Waypoint mobility model (RWP) [17] (see Fig. 2). This model

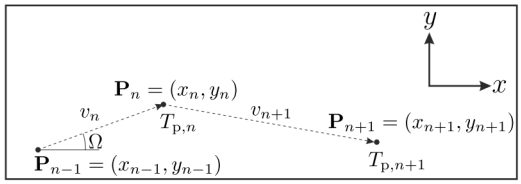

Fig. 2: Random Waypoint mobility model.

is a commonly used mobility pattern in network simulations that characterizes the random movement of nodes within a specified area. It is defined by a sequence of waypoints, where nodes move from one waypoint to another with randomly chosen speeds and directions. In the RWP model, each node begins by staying stationary at a randomly chosen initial location. Upon commencing movement, the node selects a random destination within the boundary of the simulation area and travels towards it with a velocity uniformly distributed between a predefined minimum and maximum speed. Upon reaching the destination, the node pauses for a specified time, chosen from a pre-determined probability distribution, before selecting a new destination and repeating the process.

Formally, the RWP Mobility model can be described by the tuple $(P_n, v_n, \theta_n, T_{p,n})$, where $P_n = (x_n, y_n)$ represents the coordinates of the n^{th} Waypoint. Also v_n and Ω_n are, respectively, the speed and the direction (with respect to a global reference) of the node moving towards the n^{th} waypoint. Thus, $T_{p,n}$ is the pause time at the n^{th} Waypoint before moving towards the next Waypoint. Figure 2 shows an example for the GU progresses from a random Waypoint $P_{n-1} = (x_{n-1}, y_{n-1})$ to the subsequent destination $P_n = (x_n, y_n)$, moving at a speed v_n, which is sampled from a velocity distribution $f(v)$. Subsequent to arrival, the UE pauses for a duration $T_{p,n}$, drawn from a pause-time distribution f_{Tp}. The distance traversed during each movement, D_n, is the Euclidean norm between Waypoints P_{n-1} and P_n.

B. Channel Model

Considering the probability of LoS and/or NLoS occurrence, the channel path loss between the i^{th} UAV and the j^{th} GU is given by [18]

$$PL_{ij} = \begin{cases} PL_{ij,\mathrm{los}} = \eta_{\mathrm{los}} \left(\frac{4\pi f}{c}\right)^2 d_{ij}^2, & \text{with LoS} \\ PL_{ij,\mathrm{nlos}} = \eta_{\mathrm{nlos}} \left(\frac{4\pi f}{c}\right)^2 d_{ij}^2, & \text{with NLoS} \end{cases} \quad (1)$$

where η_{los} and η_{nlos} represent the attenuation factors for LoS and NLoS links respectively. Also f and c denote for the carrier frequency and the speed of light, respectively. Thus, d_{ij} is the corresponding distance and is obtained by

$$d_{ij} = \sqrt{(X_i - X_j)^2 + (Y_i - Y_j)^2 + (H_i - H_j)^2}. \quad (2)$$

The likelihood of establishing a LoS connection is given as

$$p_{\mathrm{los}}(r) = \frac{1}{1 + a \exp(-b(\theta - a))}, \quad (3)$$

where a and b are environment-dependent constants, θ is the elevation angle, computed by $\theta = \frac{180}{\pi} \tan^{-1}\left(\frac{H}{r}\right)$, and r is

the horizontal distance between the UAV and the user. The complement, $p_{\text{nlos}}(r) = 1 - p_{\text{los}}(r)$, gives the NLoS probability. Consequently, we define the average path loss as follows:

$$\bar{PL}_{ij} = p_{\text{los}} PL_{ij,\text{los}} + (1 - p_{\text{los}}) PL_{ij,\text{nlos}}. \tag{4}$$

Therefore, the received power from i^{th} UAV at j^{th} GU's location is given by [19]:

$$P_{r_{ij}}(\text{dB}) = \begin{cases} P_t + G_{\text{3dB}} - PL_{ij,los}^{(\text{dB})} - \vartheta_{\text{LoS}}, & \text{LoS link}, \\ P_t + G_{\text{3dB}} - PL_{ij,los}^{(\text{dB})} - \vartheta_{\text{NLoS}}, & \text{NLoS link}, \end{cases} \tag{5}$$

where $P_{r_{ij}}$ and P_t are the received power at GU and transmit power at UAV, respectively. G_{3dB} is the UAV antenna gain in dB. Assuming a directional antenna with half beamwidth of θ_B [20], this gain can further be approximated as $G_{\text{3dB}} \approx \frac{29000}{\theta_B^2}$. Also, $\vartheta_{\text{LoS}} \sim \mathcal{N}(\mu_{\text{LoS}}, \sigma^2_{\text{LoS}})$ and $\vartheta_{\text{NLoS}} \sim \mathcal{N}(\mu_{\text{NLoS}}, \sigma^2_{\text{NLoS}})$ are shadow fading with normal distribution in dB scale for LoS and NLoS links, respectively. The mean and variance of the shadow fading for LoS and NLoS links are $(\mu_{\text{LoS}}, \sigma^2_{\text{LoS}})$, and $(\mu_{\text{NLoS}}, \sigma^2_{\text{NLoS}})$. The variance depends on the elevation angle and environment as follows [20]:

$$\sigma_{\text{LoS}}(\theta_j) = k_1 \exp(-k_2 \theta_j), \tag{6}$$

$$\sigma_{\text{NLoS}}(\theta_j) = g_1 \exp(-g_2 \theta_j), \tag{7}$$

where k_1, k_2, g_1, and g_2 are environmental-based constants.

III. Performance Analysis

To evaluate the system's efficiency, we consider different key metrics, including bit error rate (BER), sum rate, and energy consumption. In addition, a closed-form expression for the coverage probability at a target BER, $P_{e_{\text{th}}}$, is developed.

A. Bit Error Rate (BER)

For $\mathcal{K}$-ary PAM modulation scheme, the BER at j^{th} GU is formulated as [21]:

$$P_e = \frac{2(K-1)}{K \log_2(K)} Q\left(\sqrt{\frac{6}{(K-1)(2K-1)} \gamma_j}\right), \tag{8}$$

where K represents the modulation order, and $Q(\cdot)$ is the Q-function. Also, γ_j is the signal-to-interference-plus-noise ratio at j^{th} GU. It is given by

$$\gamma_j = \frac{P_{r_{ij}}}{\sum_{i' \in M, i' \neq i} P_{r_{i'j}} + N_0}, \tag{9}$$

where $P_{r_{ij}}$ represents the received power from UAV i to GU j, and N_0 denotes the noise power.

B. Sum Rate

The sum rate, R_m, quantifies the total data transmission rate across all users within the coverage area and is given by

$$R_m = \sum_{j=1}^{N} R_j, \tag{10}$$

where R_j represents the data rate for j-th GU, given by

$$R_j = B \cdot \log_2(1 + \gamma_j), \tag{11}$$

where B denotes for the system bandwidth.

C. Energy Consumption of UAVs

For UAVs in full-speed, the transition power is denoted as ρ_{full}. The UAV's velocity v influences its travel time, $\frac{D}{v}$, from start to endpoint, where D is the total distance traveled by the UAV. The energy consumption due to movement (E_m) and the hovering power (ρ_{hov}) are respectively given by [22]

$$E_m = \frac{D(\rho_{\text{hov}} + \rho_{\text{full}})}{v}, \tag{12}$$

$$\rho_{\text{hov}} = \sqrt[3]{\frac{(m_{\text{UAV}} \cdot g)^3}{2\pi r_u^2 N_u \kappa}}, \tag{13}$$

where m_{UAV}, g, r_u, N_u, and κ correspond to the UAV's mass, the earth gravity, the radius of propellers, the propellers numbers, and the air density, respectively.

D. Coverage Probability

In this part, a closed-form expression for the coverage probability at a target BER threshold is derived. In a noisy channel, a j^{th} user is considered belonging to the communication area of a UAV when the BER at this user is below a predefined threshold $P_{e_{\text{th}}}$. This threshold is also the value to assess the quality of the channel between the user and UAV. The coverage probability, P_c, is expressed as:

$$P_c = \mathbb{P}(P_e \leq P_{e_{\text{th}}}), \tag{14}$$

where $\mathbb{P}$ denotes the probability that the BER (P_e) falls below the threshold $P_{e_{\text{th}}}$. Substituting about P_e from (8) in (14), P_c is re-written as (15).

By re-arranging (15), it can be given as (16). Note, (15) and (16) are given at the bottom of this page.

By replacing $P_{r_{ij}}$ from (5) and re-arranging, P_c can be reformulated by (17), shown at the top of the next page. The final expression for the coverage probability is obtained by (18) shown at the top of the next page.

$$P_c = \mathbb{P}\left[\frac{2(K-1)}{K \log_2(K)} Q\left(\sqrt{\frac{6}{(K-1)(2K-1)} \frac{P_{r_{ij}}}{\sum_{i' \in M, i' \neq i} P_{r_{i'j}} + N_0}}\right) \leq P_{e_{\text{th}}}\right]. \tag{15}$$

$$P_c = \mathbb{P}\left[\frac{P_{r_{ij}}}{\sum_{i' \in M, i' \neq i} P_{r_{i'j}} + N_0} \geq \frac{(K-1)(2K-1)}{6} \left(Q^{-1}\left(\frac{K \log_2(K)}{2(K-1)} P_{e_{\text{th}}}\right)\right)^2\right]. \tag{16}$$

$$P_c = \mathbb{P}\left[\vartheta \leq P_t + G_{\text{3dB}} - \bar{PL}_{ij}^{(\text{dB})} - \left(\frac{(K-1)(2K-1)}{6} \times \left(Q^{-1}\left(\frac{K\log_2(K)}{2(K-1)}P_{e_{\text{th}}}\right)\right)^2\right) \times \left(\sum_{i'\in M, i'\neq i} P_{r_{i'j}} + N_0\right)\right]. \tag{17}$$

$$\begin{aligned} P_c =& p_{\text{los}} Q\left(\frac{PL_{ij,\text{los}} + \left(\frac{(K-1)(2K-1)}{6} \times \left(Q^{-1}\left(\frac{K\log_2(K)}{2(K-1)}P_{e_{\text{th}}}\right)\right)^2\right) \times \left(\sum_{i'\in M, i'\neq i} P_{r_{i'j}} + N_0\right) - P_t - G_{\text{3dB}} + \mu_{\text{LoS}}}{\sigma_{\text{LoS}}}\right) \\ &+ p_{\text{nlos}} Q\left(\frac{PL_{ij,\text{nlos}} + \left(\frac{(K-1)(2K-1)}{6} \times \left(Q^{-1}\left(\frac{K\log_2(K)}{2(K-1)}P_{e_{\text{th}}}\right)\right)^2\right) \times \left(\sum_{i'\in M, i'\neq i} P_{r_{i'j}} + N_0\right) - P_t - G_{\text{3dB}} + \mu_{\text{NLoS}}}{\sigma_{\text{NLoS}}}\right). \end{aligned} \tag{18}$$

Based on the derived coverage probability in (18), coverage is quantified in terms of the number of GUs effectively covered by UAV$_i$. Consequently, this leads to a binary decision formulation, which is expressed as follows.

$$C_j^i = \begin{cases} 1, \text{ if GU } j \text{ is covered by one UAV} - i \\ 0, \text{ otherwise} \end{cases}. \tag{19}$$

IV. System Optimization

A. Problem Formulation

The primary objective is to optimize the UAV's 3D deployment for maximal coverage and sum rate, and minimal power consumption while ensuring the system reliability and mobility. To formulate the problem under consideration, a joint multi-objective optimization problem is proposed as follows:

$$\max\left(w_1 \times \sum_{j=1}^{M} C_j^i + w_2 \times R_m - w_3 \times E_m\right), \tag{20}$$

Subject to:

$$\textbf{C1: } P_{e_j} \leq P_{e_{\text{th}}}, \quad \forall j \in \{1, 2, \cdots, M\}, \tag{21a}$$

$$\begin{aligned} \textbf{C2: } & X_{\min} \leq X_i \leq X_{\max}, \\ & Y_{\min} \leq Y_i \leq Y_{\max}, \\ & H_{\min} \leq H_i \leq H_{\max}, \quad \forall i \in \{1, 2, \cdots, N\}, \end{aligned} \tag{21b}$$

$$\textbf{C3: } E_{m_i} \leq E_{m_{\text{th}}}, \quad \forall i \in \{1, 2, \cdots, N\}. \tag{21c}$$

It is shown in (20) that three performance metrics are optimized as follows. ***i***) Maximizing the coverage, ***ii***) Maximizing the sum rate, and ***iii***) Minimizing the energy consumption. In addition to, the constraint in (21a) is imposed to ensure the reliability of the system (**a) Error rate constraint**). In other words, each user should maintain an adequate error rate value lower than a predetermined threshold, denoted as $P_{e_{\text{th}}}$. Also, the constraint in (21b) is required to ensure that each UAV operate/move within designated 3D spatial limits (**b) 3D spatial limits constraint**). Finally, the constraint in (21c) is included in order to choose from the feasible solutions which ensure that each UAV's energy consumption does not exceed a predefined threshold denoted by $E_{m_{th}}$ (**c) Energy constraint**).

B. Problem Solving

To efficiently and accurately solve the optimization problem under consideration, a novel optimization algorithm is proposed which integrates the BO with a chaotic map. In the following, the two key components (i.e., BO and chaotic map) used in the proposed approach are first illustrated. Then, we explain the proposed improved CBO algorithm.

1) Bonobo Optimizer (BO): The Bonobo Optimization (BO) algorithm, as introduced by Das and Pratihar in 2019 [23], represents one of the most contemporary meta-heuristics. BO draws inspiration from the intricate social behaviors and reproductive strategies observed in bonobos. Bonobos exhibit a unique fission-fusion social structure, where they split into smaller groups for various activities and then come together for communal tasks. This algorithm models a population of solutions as "Bonobos," with the best-performing solution termed as α_{bo}. The algorithm operates through two main phases: the positive phase (P_p), which is triggered by improvements in the fitness value of α_{bo}, indicating progress towards optimal solutions; and the negative phase (N_p), initiated when there is no improvement, signifying stagnation. Key parameters within this framework include the Positive Phase Count (ppc) and Negative Phase Count (npc), which track the consecutive iterations of improvement or stagnation, respectively, guiding the optimization process efficiently.

For mating, the process selects the p-th bonobo for mating with the i-th bonobo by leveraging the bonobos' natural fission-fusion social dynamics, where temporary subgroups are formed to evaluate fitness for mating. The maximum number of individuals in each subgroup, $tsgs_{max}$, is calculated using the equation $tsgs_{max} = \max(2, tsgs_{factor} \times Ns)$, where Ns is the total population size and $tsgs_{factor}$ is a predetermined factor affecting subgroup size. Fitness is assessed within each subgroup, and the member with the highest fitness is compared to the i-th bonobo. If this member (the potential p-th bonobo) has higher fitness, it is chosen for mating; otherwise, a random member from the subgroup is selected. This may result in selecting of alpha bonobo (α_{bo}) as p-th bonobo, emphasizing the preference for mating with individuals of higher fitness.

The BO algorithm utilizes four mating strategies, namely promiscuous, consortship, restrictive, and extra group mating, to generate new bonobos. The selection of a mating strategy depends on the phase condition during the current iteration. The phase probability is used to determine the mating strategy. A new bonobo is formed in the positive phase if a randomly generated number r_1 lower or equal the value of P_p. The initial value of P_p is set to 0.5. Eq. (22) describes the formation of a new bonobo during the positive phase:

$$\begin{aligned} new\_bo_j = & bo_j^i + R_1 \cdot scab \cdot (\alpha_j^{bo} - bo_j^i) \\ & + (1 - R_1) \cdot scsb \cdot \text{flag} \cdot (bo_j^p - bo_j^i), \end{aligned} \tag{22}$$

where new_bo_j and α_j^{bo} represent the i-th variable of the newly formed individual and the alpha individual, respectively. The coefficients $scab$ and $scsb$ stand for sharing coefficients, R_1 is a uniformly distributed random number in the interval [0, 1], and flag indicates the chosen mating strategy, with 1 representing promiscuous and -1 indicating restrictive.

During the negative phase, the choice between consortship and extra-group mating strategies is made through a random selection process. This decision is guided by a random variable denoted as (r_2). Consortship is selected over extra-group mating when r_2 exceeds the probability of extra group mating (P_{xgm}). Under these conditions, the new bonobo's formation is determined by

$$new\_bo_j = \begin{cases} bo_j^i + \text{flag} \times e^{-r_5} \times (bo_j^i - bo_j^p), \\ \qquad\qquad \text{if flag} = 1 \| r_6 \leq P_d \\ bo_j^p, \qquad \text{otherwise} \end{cases}, \tag{23}$$

where, r_5 and r_6 are random numbers in [0, 1] and P_d is the directional probability. In the case of extra group mating, the equation for bonobo formation are the following:

$$\beta 1 = e(r_4^2 + r_4 - 2/r_4). \tag{24}$$

$$\beta 2 = e(-r_4^2 + 2r_4 - 2/r_4). \tag{25}$$

$$new\_bo_j = bo_j^i + \beta 1 \times (Var\_max_j - bo_j^i). \tag{26}$$

$$new\_bo_j = bo_j^i + \beta 2 \times (bo_j^i - Var\_min_j). \tag{27}$$

$$new\_bo_j = bo_j^i + \beta 1 \times (bo_j^i - Var\_min_j). \tag{28}$$

$$new\_bo_j = bo_j^i + \beta 2 \times (Var\_max_j - bo_j^i). \tag{29}$$

In these equations, $\beta 1$ and $\beta 2$ are intermediate parameters for calculating new_bo_j with r_4 is a random number in [0, 1] and $r_4 \neq 0$. Var_min_j and Var_max_j are the lower and upper boundaries of the j-th variable. More specific conditions of the application of these equations are in [23]. At the end of each iteration cycle, the fitness values and optimization parameters of the bonobo community are updated.

2) Chaotic Map: The concept of chaotic maps is utilized in optimization to leverage the inherent randomness and deterministic chaos of nonlinear systems for enhancing algorithm performance. These maps, characterized by randomness, ergodicity, and non-repetition behavior, can replace random initialization in meta-heuristic algorithms, potentially improving convergence rates and preventing stagnation in local optima. Among various chaotic maps, the Sine map is particularly valued for its ability to generate uniform initial values between 0 and 1, thus accelerating the optimization process. This approach is applied to replace random variables in algorithms, as described by the following equation:

$$z_{t+1} = \frac{\alpha}{4} \sin(\pi z_t), \tag{30}$$

where z_{t+1} is the value at the next iteration, z_t is the current value, and $\alpha \in [0, 4]$ is a constant parameter.

3) Proposed Solution: CBO: In this part, we present the structure of our proposed CBO algorithm, which aims to enhance the optimization performance of the original Bonobo Optimizer (BO) by incorporating a chaotic map. Our tailored version of the BO algorithm addresses the problem of UAV placement within dynamic networks, with the objective of achieving maximum coverage and minimal energy consumption. The key modifications we have made to the BO algorithm are as follows:

- **Enhanced Initial Mating Probability:** We've refined our strategy to favor the exploitation phase over exploration, targeting more energy-efficient solutions. By updating the initial extra-group mating probability from 0.5 to 0.9, we focus on improving existing solutions rather than venturing into new territories. This adjustment ensures better stability and energy savings throughout the optimization process.
- **Efficient Starting Point (Initial UAV Placement):** We employ the original BO algorithm to generate the initial positions of UAVs, taking into account the objectives of maximizing coverage and rate. It is worth noting that the quality of the initial positions can significantly impact the optimization outcome.
- **Chaotic Sine Map Integration:** To enhance the stochastic behavior of the BO algorithm, we integrate a chaotic sine map. By generating a random number, denoted as r_1, using the sine chaotic map based on (30), the algorithm focuses on exploiting solutions near the current solution.

TABLE I. Simulation Parameters

Parameter	Value	Parameter	Value
P_t	30 dBm	G_{3dB}	4.53 dB
k_1	10.39	k_2	0.05
g_1	29.06	g_2	0.03
f	2 GHz	a	9.6
b	0.16	η_{los}	1
η_{nlos}	20	θ_B	80°
K	2	B	10 MHz
N_0	10^{-15}	w_1	0.6
w_2	0.2	w_3	0.2
$P_{e_{\text{th}}}$	10^{-6}	α	4
z_0	0.7		

V. Numerical Results and Discussions

In this section, we present the numerical results obtained from our proposed algorithm considering the simulation pa-

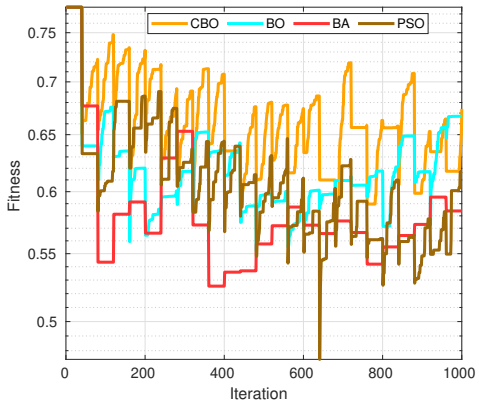

(a)

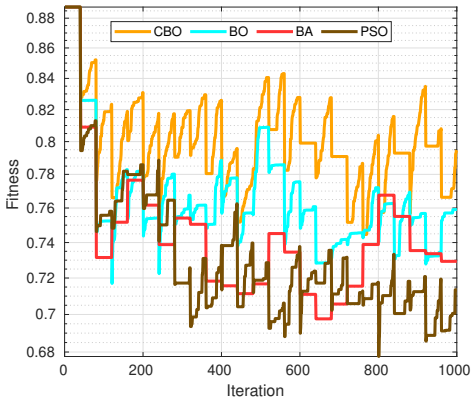

(b)

Fig. 3: Fitness for (a) Scenario 1 (b) Scenario 2.

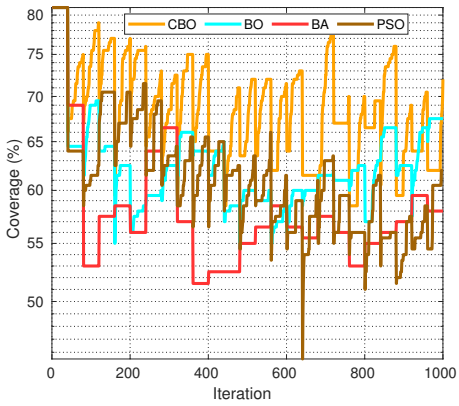

(a)

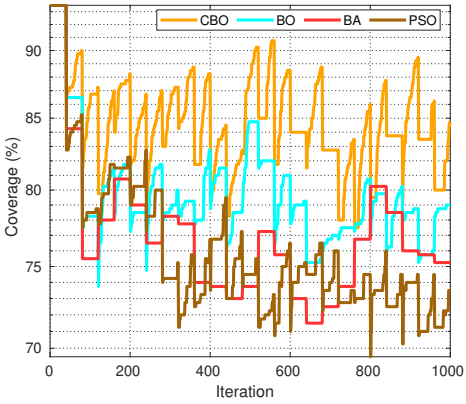

(b)

Fig. 4: Coverage for (a) Scenario 1 (b) Scenario 2.

rameters shown in Table I and given in [23], [24]. The simulations are conducted in a 2000 $\times$ 2000 m^2 area. The user distributions are assumed to follow the RWP model and they change every 40 iterations to capture dynamic scenarios. To ensure reliable results, we run 1000 iterations and average the outcomes over 20 executions, mitigating the effects of randomness. We evaluate the performance of our proposed algorithm in two distinct scenarios: **Scenario 1**, which consider 200 users and 20 UAVs, and **Scenario 2**, which involve 400 users and 30 UAVs. Our analysis focuses on assessing the algorithm's effectiveness in terms of Coverage, Sum Rate, and Fitness. To demonstrate the superiority of our proposed approach, we conduct a comparative study against the original BO, BA, and PSO algorithms.

In Fig. 3, the fitness results for all the algorithms under consideration are depicted. It is evident that the proposed CBO algorithm consistently outperforms the other algorithms across various user distributions for both scenarios. Specifically, consider iteration t = 200 and scenario 1, the CBO algorithm achieves a fitness value of 0.73. In comparison, the fitness values for the BO, PSO, and BA are 0.62, 0.69, and 0.57, respectively. Moreover, at iteration t = 580 and scenario 2, the recorded fitness values are 0.845, 0.785, 0.69, and 0.745 for the CBO, BO, PSO, and BA algorithms, respectively.

In Fig. 4, the coverage results for all considered algorithms across both scenarios are presented. Notably, the proposed CBO algorithm consistently demonstrates the highest coverage percentage for all user distributions in both scenarios. For instance, let's examine scenario 1 at iteration t = 700. The total achieved coverage for CBO is 78%, showcasing improvements of 16%, 15%, and 20% compared to BO, PSO, and BA, respectively. Similarly, in scenario 2 at t = 400, the coverage percentages are 88%, 83%, 77%, and 74% for CBO, BO, PSO, and BA, respectively.

Fig. 5 presents a comparative performance analysis of the considered algorithms in terms of sum rate for both scenarios. The analysis reveals that the CBO algorithm exhibits rapid initial improvement, surpassing the other methods (BO, PSO, and BA) and achieving a higher sum rate earlier in the optimization process. This observation suggests that CBO may possess an advantageous exploratory capability, enabling it to escape rapidly from local optima. For instance, at t = 320 in scenario 1, the CBO algorithm achieves a sum rate of 200 Mbit/s. This represents an improvement of 90 Mbit/s, 150 Mbit/s, and 159 Mbit/s compared to BO, PSO, and BA algorithms, respectively. Furthermore, consider scenario 2 and t = 200, the achieved sum rate are 640 Mbit/s, 500 Mbit/s, 210 Mbit/s, and 180 Mbit/s for CBO, BO, PSO, and BA, respectively.

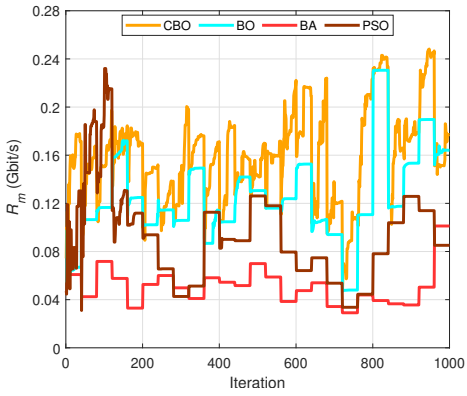

(a)

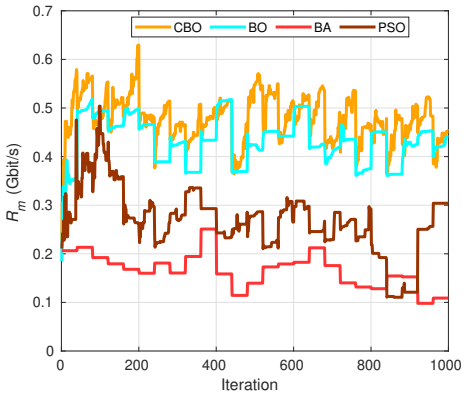

(b)

Fig. 5: Sum rate for (a) Scenario 1 (b) Scenario 2.

VI. Conclusion

In this paper, we have focused on the 3D optimal deployment of multiple UAVs in dynamic scenarios, with a particular emphasis on the adoption of the RWP mobility model for simulating realistic user movements. A closed-form expression for the achievable coverage probability at targeted error rate performance has been derived considering the probabilistic LoS and NLoS links. Based on that, a multi-objective optimization problem has been formulated that seeks to balance the maximization of network coverage and sum rate with the minimization of UAV power consumption, acknowledging the inherent trade-offs between the objectives and constraints. To address the complexity of this problem, a novel enhanced CBO algorithm has been proposed, which takes the advantages of both the chaotic maps and the BO algorithm to enhance optimization efficiency and accuracy. The obtained results demonstrate that the proposed CBO algorithm significantly outperforms traditional optimization techniques such as the BO, PSO, and BA schemes.

References

[1] X. Deng *et al.*, "Detecting confident information coverage holes in industrial internet of things: An energy-efficient perspective," *IEEE Commun. Mag.*, vol. 56, no. 9, pp. 68–73, 2018.

[2] S. A. Al-Ahmed *et al.*, "Optimal 3D UAV base station placement by considering autonomous coverage hole detection, wireless backhaul and user demand," *J. Commun. Netw.*, vol. 22, no. 6, pp. 467–475, 2020.

[3] M. Alzenad *et al.*, "3-D placement of an unmanned aerial vehicle base station (UAV-BS) for energy-efficient maximal coverage," *IEEE Wirel. Commun. Lett.*, vol. 6, no. 4, pp. 434–437, 2017.

[4] ——, "3-D placement of an unmanned aerial vehicle base station for maximum coverage of users with different QoS requirements," *IEEE Commun. Lett.*, vol. 7, no. 1, pp. 38–41, 2017.

[5] Y. Chen *et al.*, "Optimum placement of UAV as relays," *IEEE Commun. Lett.*, vol. 22, no. 2, pp. 248–251, 2017.

[6] M. Mozaffari *et al.*, "Mobile internet of things: Can UAVs provide an energy-efficient mobile architecture?" in *2016 IEEE Glob. Commun. Conf. (GLOBECOM)*. IEEE, 2016, pp. 1–6.

[7] S. Kumar *et al.*, "Backhaul and delay-aware placement of UAV-enabled base station," in *IEEE INFOCOM 2018-IEEE Conf. Comput. Commun. Workshops. (INFOCOM WKSHPS)*. IEEE, 2018, pp. 634–639.

[8] M. Mozaffari *et al.*, "Drone small cells in the clouds: Design, deployment and performance analysis," in *2015 IEEE Glob. Commun. Conf. (GLOBECOM)*. IEEE, 2015, pp. 1–6.

[9] A. Al-Hourani *et al.*, "Optimal LAP altitude for maximum coverage," *IEEE Wirel. Commun. Lett.*, vol. 3, no. 6, pp. 569–572, 2014.

[10] M. Mozaffari *et al.*, "Unmanned aerial vehicle with underlaid device-to-device communications: Performance and tradeoffs," *IEEE Trans. Wirel. Commun.*, vol. 15, no. 6, pp. 3949–3963, 2016.

[11] M. M. Azari *et al.*, "Joint sum-rate and power gain analysis of an aerial base station," in *2016 IEEE Globecom Workshops (GC Wkshps)*. IEEE, 2016, pp. 1–6.

[12] V. V. Chetlur *et al.*, "Downlink coverage analysis for a finite 3-D wireless network of unmanned aerial vehicles," *IEEE Trans. Commun.*, vol. 65, no. 10, pp. 4543–4558, 2017.

[13] C. Di Franco *et al.*, "Energy-aware coverage path planning of UAVs," in *2015 IEEE Int. Conf. Auton. Robot Syst. Compet.* IEEE, 2015, pp. 111–117.

[14] K. Li *et al.*, "Energy-efficient cooperative relaying for unmanned aerial vehicles," *IEEE Trans. Mob. Comput.*, vol. 15, no. 6, pp. 1377–1386, 2015.

[15] J. Zhang *et al.*, "Spectrum and energy efficiency maximization in UAV-enabled mobile relaying," in *2017 IEEE Int. Conf. Commun. (ICC)*. IEEE, 2017, pp. 1–6.

[16] A. Trotta *et al.*, "Fly and recharge: Achieving persistent coverage using small unmanned aerial vehicles (SUAVs)," in *2017 IEEE Int. Conf. Commun. (ICC)*. IEEE, 2017, pp. 1–7.

[17] E. Hyytia *et al.*, "Spatial node distribution of the random waypoint mobility model with applications," *IEEE Trans. Mob. Comput.*, vol. 5, no. 6, pp. 680–694, 2006.

[18] X. Li *et al.*, "A near-optimal UAV-aided radio coverage strategy for dense urban areas," *IEEE Trans. Veh. Technol.*, vol. 68, no. 9, pp. 9098–9109, 2019.

[19] A. Al-Hourani *et al.*, "Modeling air-to-ground path loss for low altitude platforms in urban environments," in *2014 IEEE Glob. Commun. Conf.* IEEE, 2014, pp. 2898–2904.

[20] M. Mozaffari *et al.*, "Efficient deployment of multiple unmanned aerial vehicles for optimal wireless coverage," *IEEE Commun. Lett.*, vol. 20, no. 8, pp. 1647–1650, 2016.

[21] F. Zhou *et al.*, "Two-dimensional new communication technology for networked ammunition," *IEEE Access*, vol. 8, pp. 133 725–133 733, 2020.

[22] H. Hu *et al.*, "Optimization of energy management for UAV-enabled cognitive radio," *IEEE Wirel. Commun. Lett.*, vol. 9, no. 9, pp. 1505–1508, 2020.

[23] A. K. Das *et al.*, "A new bonobo optimizer (BO) for real-parameter optimization," in *2019 IEEE Reg. 10 Symp.(TENSYMP)*. IEEE, 2019, pp. 108–113.

[24] S. M. Taleb *et al.*, "Solving the mesh router nodes placement in wireless mesh networks using coyote optimization algorithm," *IEEE Access*, vol. 10, pp. 52 744–52 759, 2022.

VII. Acknowledgment

The authors gratefully acknowledge support for this work from The Arctic University of Norway and the EU Interreg Aurora program through the HE4T project, as well as from the Regional STIMULE CORTESE Project of the Hauts-de-France Region.